Proton-loaded zeolites. 2. Dehydrohalogenation versus decationization kinetics: Cation and acidity effects

ARTICLE *in* THE JOURNAL OF PHYSICAL CHEMISTRY · OCTOBER 1990

Impact Factor: 2.78 · DOI: 10.1021/j100384a054

3 AUTHORS, INCLUDING:

Saim Özkar
Middle East Technical University
298 PUBLICATIONS **5,295** CITATIONS

SEE PROFILE

Lisa Mcmurray
Royal Ottawa Mental Health Centre; Universit…
10 PUBLICATIONS **85** CITATIONS

SEE PROFILE

Proton-Loaded Zeolites. 2. Dehydrohalogenation versus Decationization Kinetics: Cation and Acidity Effects

Geoffrey A. Ozin,* Saim Özkar,† and Lisa McMurray

Lash Miller Chemistry Department, University of Toronto, 80 St. George St., Toronto, Ontario, Canada M5S 1A1 *(Received: February 20, 1990; In Final Form: May 4, 1990)*

The work presented in part 1 of this study established that the sorption of anhydrous HX into dehydrated $Na_{56}Y$ progresses through a sequence of steps involving HX ionization and charge separation, oxygen framework protonation, formation of α-cage confined cation-anion contact ion pairs, and proton solvation by HX. A logical extension, which is the subject of this study, concerns the effect of extraframework alkali metal cation type ($M = Li^+$, Na^+, K^+, Rb^+, Cs^+) on the sorption process. The question of the acidity of proton-loaded zeolites compared to Brønsted acid zeolites is addressed by using probe reactions with weak bases like ethane and cyclopropane. Additional insight into these systems is also obtained from a quantitative comparison of the kinetic and thermodynamic activation parameters for the dehydrohalogenation of proton-loaded zeolites exemplified by $(HX)_8Na_{56}Y$ relative to the decationization (dehydroxylation) of Brønsted acid zeolites represented by $H_8Na_{48}Y$.

Introduction

Brønsted acid sites in zeolite Y are most commonly created by ammonium ion exchange of a predetermined number of Na^+ cations in the parent $Na_{56}Y$ followed by a thermal vacuum deammination procedure:[1-3]

$$Na_{56}Y \rightarrow (NH_4)_nNa_{56-n}Y \rightarrow H_nNa_{56-n}Y$$

In this series of steps, specific extraframework Na^+ cation sites are replaced by ammonium cations which, on giving up ammonia, serve to target the charge-balancing protons to specific oxygen framework sites. The juxtaposition of cations and protons as a function of n has been studied in detail as described earlier.[3,4] The central point here is that charge balance is strictly maintained and protons replace Na^+ cations on a one-to-one basis. As a result of this gradual interconversion of charge-balancing ions, the Sanderson average electronegativity S_{int} of the zeolite[3] is expected to change as there is a significant difference in S_{int} between the end members:

$$S_{int}(Na_{56}Y) = 3.6 \qquad S_{int}(H_{56}Y) = 4.1$$

These Sanderson electronegativities imply that the electron density on the oxygens in $Na_{56}Y$ is higher than that in the fully Brønsted acid form, and one therefore expects this change to be manifest in the binding strength of the proton (or indeed any charge-balancing cation) to its lattice oxygen site.

In contradistinction to the traditional technique of producing Brønsted acid sites in zeolite Y through deammination of $(NH_4)_nNa_{56-n}Y$, the methodology of directly protonating zeolite Y through the room-temperature reaction with anhydrous HX must be considered as being quite distinct:

$$H_nNa_{56-n}Y + mHX \rightarrow \{mX^-Na^+\}\{H_nNa_{56-n-m}Y\}\{H'_mY\}$$

The model expounded for this process in part 1 of this study implicates extraframework cations in the act of polarizing, ionizing, and charge-separating the dipolar sorbate HX into its two constituent parts. The end product is envisaged to be a structurally intact zeolite Y *in which the original Na^+ cation distribution* remains essentially undisturbed (FT-far-IR cation probe), the halide anion is associated with α-cage Na^+ cations as weakly bonded contact ion pairs, and the released proton is targeted to unoccupied, specific oxygen framework sites in both the α- and β-cages of the host lattice. As the amount of HX molecules is increased, this situation is disturbed by an equilibrium process best described as selective α-cage solvation of the proton by HX, as outlined in part 1 of this study.

A pivotal question that one must now address is whether or not the protonated oxygen framework sites denoted ZOH' in proton-loaded zeolites are in some way different from the normal Brønsted acid sites denoted ZOH. To gain some preliminary insight into this problem, we will examine the (a) bond strengths, (b) acidities, (c) solvation, and (d) H/D isotope exchange properties of these two kinds of protons.

(*a*) *Bond Strengths.* This physical characteristics of ZOH and ZOH' can be viewed through two enlightening experiments. First is the comparison of ν(OH) for $(HX)_8Na_{56}Y$ with $H_8Na_{48}Y$ and $H_{16}Na_{40}Y$. As can be deduced from an examination of Figures 6 and 7 (part 1), the frequencies for both α- and β-cage protons between samples are essentially identical. Second is the comparison of ν(OH) for $H_8Na_{48}Y$ and $H_{16}Na_{40}Y$ with their protonated counterparts $(HX)_mH_8Na_{48}Y$ and $(HX)_mH_{16}Na_{40}Y$, respectively. As can be inferred again from inspection of Figures 6 and 7 (part 1), the frequencies for both α- and β-cage protons between samples are essentially indistinguishable. Clearly, the vibrational frequencies and bond stretching force constants for the two ZOH and ZOH' oscillators are indistinguishable. As bond stretching force constants for essentially decoupled high-frequency ν(OH) oscillators reflect the curvature and hence the depth of the OH potential, it is reasonable to conclude that ZOH and ZOH' have essentially identical bond strengths.

(*b*) *Acidities.* As described in part 1 of this study, the acidity of a Brønsted acid or proton-loaded zeolite oxygen framework site is only a meaningful concept in the presence of a base; that is, acidity cannot be separated from a scheme involving the interaction with molecules. In the case of ZOH bonds, any charge transfer from the donor molecule to the proton (acceptor) will result in a weakening of the OH bond. The weakening of the OH bond upon adsorption, including the differences in sensitivity to the interaction with different molecules, as measured by changes in the bathochromic shift of the frequency of the OH stretching vibration, is a sensitive and convenient technique for evaluating the acidity of the ZOH (acceptor) and the basicity of the interacting molecule (donor).[3] Using this approach, we can begin to enquire into the question of acidity of ZOH compared to ZOH'.

In order, however, to gain meaningful information on the question of acidity of ZOH versus ZOH', one must be able to actually measure a base-induced bathochromic shift on the ν(OH)/ν(OH') stretching frequencies.[3] To achieve this end, one

† On leave of absence from the Chemistry Department, Middle East Technical University, Ankara, Turkey.

(1) Breck, D. W. *Zeolite Molecular Sieves*; Wiley: New York, 1984. Barrer, R. H. *Hydrothermal Chemistry of Zeolites*; Academic Press: New York, 1982.
(2) *Zeolite Chemistry and Catalysis*; Rabo, J., Ed.; ACS Symp. Ser. No. 171; American Chemical Society: Washington, DC, 1976; p 118.
(3) Mortier, W. J.; Schoonheydt, R. A. *Prog. Solid State Chem.* **1985**, *16*, 1 and references therein.
(4) Ozin, G. A.; Baker, M. D.; Godber, J. G. *J. Phys. Chem.* **1989**, *93*, 2899 and references therein.

0022-3654/90/2094-8289$02.50/0

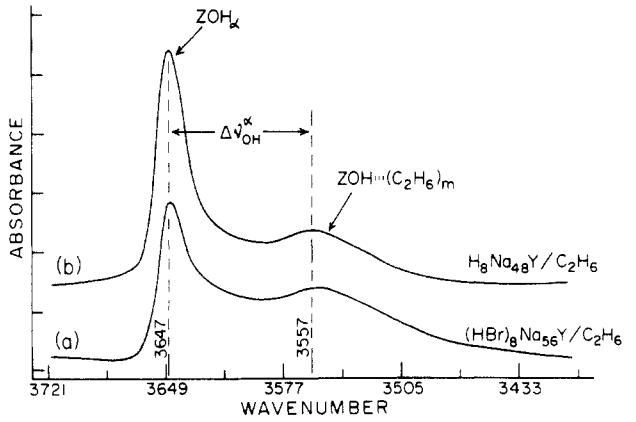

Figure 1. Mid-IR spectra of (a) $(HBr)_8Na_{56}Y/C_2H_6$ and (b) $H_8Na_{48}Y/C_2H_6$.

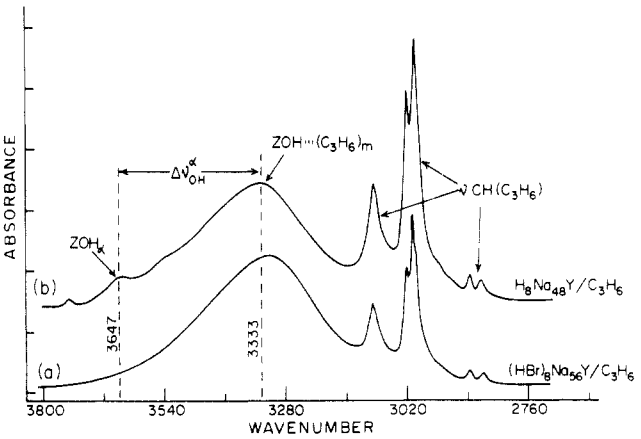

Figure 2. Mid-IR spectra of (a) $(HBr)_8Na_{56}Y/C_3H_6$ and (b) $H_8Na_{48}Y/C_3H_6$.

must choose a base B which has a sufficiently low proton affinity so as not to actually detach the proton from the oxygen framework to form the detached conjugate acid, BH^+. In this regard, alkanes prove to be ideal candidates for the task at hand. We have investigated in detail the bathochromic shifts of the series of Brønsted acid zeolites $H_nNa_{56-n}Y$ and proton-loaded zeolites $(HX)_mH_nNa_{56-n}Y$ with a large range of acyclic and cyclic alkanes, as well as halo-substituted alkanes. The details of this comprehensive study will be reported in a separate publication. For the specific immediate purpose of probing the acidity of ZOH versus ZOH′, it will be sufficient to just present our findings for ethane and cyclopropane (Figures 1 and 2). It is striking that the $\Delta\nu_{OH}^{\alpha}$ bathochromic shifts are about a factor of 4 larger for ethane ($\sim$80 cm^{-1}) than for cyclopropane ($\sim$300 cm^{-1}), presumably reflecting the expected difference in base strength between these two alkanes. This increase in the strength of interaction of the alkane with the zeolite OH group on passing from C_2H_6 to C_3H_6 is also witnessed by the expected enhancement in the bandwidth at half-height ($\Delta\nu_{1/2}$) and the intensity (I) of the red-shifted OH absorption.[5] The crucial observation for the purpose of this study, however, is the actual bathochromic shift $\Delta\nu_{OH}$, the $\Delta\nu_{1/2}$, and the I for ZOH···(alkane)$_m$ compared to ZOH′···(alkane)$_m$. They are essentially *identical* for both the ethane and cyclopropane acidity calibrators (Figures 1 and 2). These observations leave little doubt that, from the point of view of acidity, protonated oxygen framework sites, ZOH′, are essentially indistinguishable from normal Brønsted acid sites, ZOH.

(*c*) *Solvation.* In part 1 of this study we presented a compelling case for the solvation of protonated lattice sites ZOH′ (created by HX reaction with $Na_{56}Y$) with HX itself. The proposed ZOH′···$(X-H)_n$ model for this process is in essence an acid–base

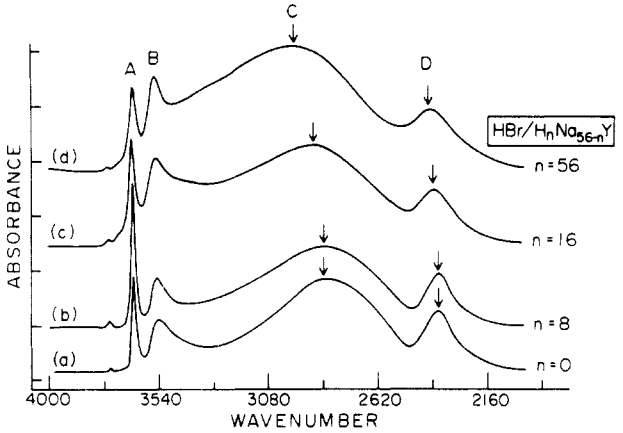

Figure 3. Mid-IR spectra of $HBr/H_nNa_{56-n}Y$: (a) $n = 0$, (b) $n = 8$, (c) $n = 16$, (d) $n = 56$.

reaction between ZOH′ and HX, analogous to those described for ZOH′···(alkane)$_m$ in the previous section of this paper. In actual fact, the frequency of the ν(OH′) C band for ZOH′···$(X-H)_n$ relative to its parent ν(OH′) in ZOH′ again represents a bathochromic shift $\Delta\nu_{OH}$ calibrator of the acid strength of the ZOH′ proton.

With this as our basic postulate, another revealing experiment for comparing the physical characteristics of ZOH′ and ZOH involves measuring the bathochromic $\Delta\nu_{OH'}$ and $\Delta\nu_{OH}$ shifts for HX solvated protons ZOH′ in $(HX)_nNa_{56}Y$ and HX solvated Brønsted acid sites ZOH in $(HX)_nH_8Na_{48}Y$, respectively. Typical results for this kind of experiment are shown in Figure 3. From inspection of the data, there remains little ambiguity that indeed, between these two samples, ZOH′ and ZOH are indistinguishable in their bond strengths as well as their acidities. The observed $\Delta\nu_{OH}$ shifts in the complete $HX/H_nNa_{56-n}Y$ series ($n = 0$–56) (Figure 3) will be discussed later.

(*d*) *H/D Isotope Exchange Properties.* It is well documented that normal Brønsted acid sites ZOH can participate in H/D isotope exchange reactions with numerous deuterated molecules such as D_2, D_2O, and ND_3.[1-4] The fairly basic D_2O and ND_3 molecules cause rapid H/D scrambling at room temperature (RT) while the weakly basic D_2 molecule requires more severe temperature conditions, usually around 400 °C for full exchange. The kinetics, mechanism, and isotope effects for the D_2/ZOH and H_2/ZOD scrambling reactions in Brønsted acid zeolites have been studied by Boudart et al.,[6] from which the most likely transition state for the exchange reaction is envisaged to be of the form

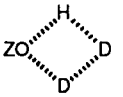

In a similar vein, the outstanding acidic and carboniogenic properties of zeolites are well appreciated, especially in the context of Brønsted acid catalyzed transformations of saturated hydrocarbons.[1-3] The H/D scrambling reactions between alkanes and the Brønsted acid sites of zeolites, like D_2/ZOH described above, can be envisaged to involve transition states of the form

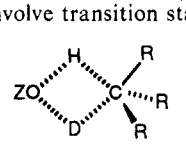

With this as minimal background, one can extract information from the H/D scrambling reactions of ZOH′ and ZOH with, for example, D_2, DX, and various deuterated alkanes to shed additional light on the nature of protonated oxygen framework sites ZOH′ relative to Brønsted acid sites ZOH. Furthermore, experiments of this type will enlighten questions concerning the

(5) Sandorfy, C. In *The Hydrogen Bond*; Schuster, P., Zundel, G., Sandorfy, C., Eds.; North-Holland: Amsterdam, 1976; Vols. I–III.

(6) Dalla Betta, R. A.; Boudart, M. *J. Chem. Soc., Faraday Trans. 1* **1976**, *72*, 1723.

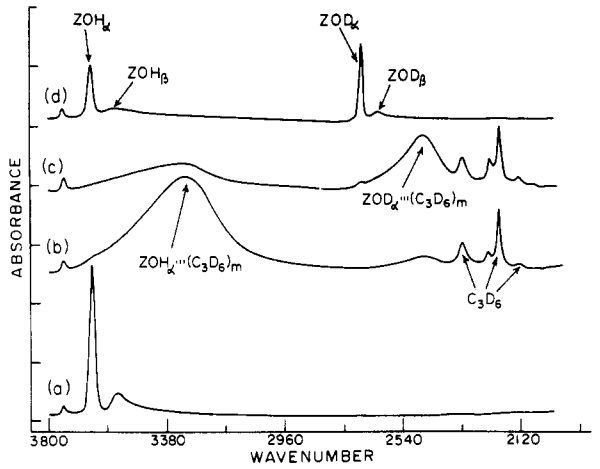

Figure 4. Mid-IR spectra of (a) $(HBr)_8Na_{56}Y$ and (b) $(HBr)_8Na_{56}Y/C_3D_6$ immediately following impregnation of 200 Torr of C_3D_6; (c) the same as (b) but after 20 h; (d) the same as (c) but after evacuation at RT.

mobility and exchange properties of protons located in the α- and β-cages of these two kinds of zeolite.

Let us first examine the RT H/D isotope exchange reaction of ZOH′ and ZOH using $(HX)_8Na_{56}Y/DX$ and $H_{16}Na_{40}Y/DX$ systems, respectively (Figures 14 and 15, part 1). Here the transition state for H/D interchange is envisaged to be of the form

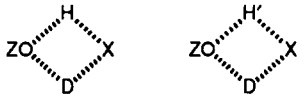

where the initial interaction is considered to be confined to α-cage ZOH′ and ZOH sites (see part 1 and earlier discussion).

The results of the aforementioned RT study are summarized in Figures 14 and 15 of part 1. One can conclude by inspection of the data that (i) H/D exchange occurs for both naked ZOH′ and ZOH sites as well as for both solvated ZOH′···$(XH)_n$ and ZOH···$(XH)_m$ species, (ii) the exchange process is rapid with essentially the same rate measured for 50% H/D exchange for both ZOH′ and ZOH, and (iii) rapid exchange occurs for both α- and β-cage ZOH′ and ZOH sites.

Again there remains little doubt from these results that protonated oxygen framework sites ZOH′ are essentially indistinguishable in their H/D exchange properties, toward DX, from those of normal Brønsted acid sites ZOH. It is interesting to note that the results shown in Figures 14 and 15 of part 1 eliminate an exchange process that is localized in the α-cage (eq 1) and instead favor a process involving an α-cage exchange followed by a rapid α–β cage switching step (eq 2) for both ZOH′ and ZOH types, as illustrated below:

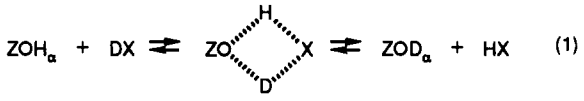

$$ZOD_\alpha + ZOH_\beta \rightleftarrows ZOH_\alpha + ZOD_\beta \quad (2)$$

These experimental observations provide compelling evidence that one is dealing with highly mobile α- and β-cage protons for both ZOH′ and ZOH types which are able to rapidly switch between α- and β-cage oxygen framework sites.

A similar state of affairs is experienced with RT H/D scrambling reactions of ZOH′ and ZOH found in the systems $(HX)_8Na_{56}Y/C_3D_6$ and $H_8Na_{48}Y/C_3D_6$. The results of this study are summarized in Figure 4. Deductions i, ii, and iii laid out above for DX-induced H/D exchanges of ZOH′ and ZOH protons apply equally well to C_3D_6-induced H/D exchanges. A similar α-cage specific H/D exchange process between ZOH/C_3D_6 (eq 3) followed by a fast ZOD_α/ZOH_β proton switching process similar to that described for DX (eq 4) again fits the experimental observations (Figure 4) as illustrated below:

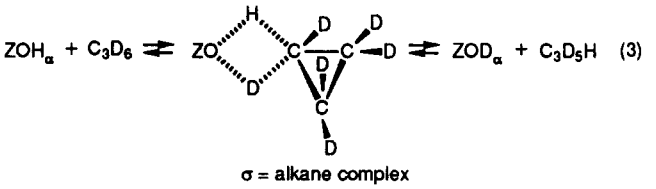

σ = alkane complex

$$ZOD_\alpha + ZOH_\beta \rightleftarrows ZOH_\alpha + ZOD_\beta \quad (4)$$

Whether or not the σ-alkane complex is in equilibrium with a small undetected concentration of a protonated alkane complex as illustrated below

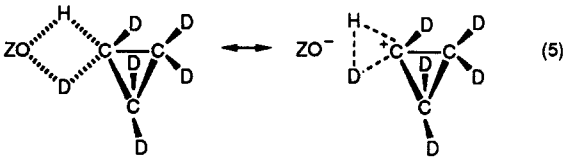

cannot be decided with the present data and forms the subject of ongoing work in our laboratory.

Another point that cannot presently be clarified by vibrational spectroscopy concerns the mechanism whereby mobile protons interchange between α- and β-cages. This enquiry is probably best addressed through dynamic proton NMR studies currently under way in our laboratory. Clearly the ZOD_α/ZOH_β exchange process strictly requires proton mobility between centers. This is not the question! What one really wishes to discover is whether or not the mere presence of an interacting molecule like DX or C_3D_6 provides the actual vehicle that causes the proton to hop from one oxygen to the next and/or whether the $\alpha \leftrightarrow \beta$ cage proton switching process can proceed unassisted without the help of a carrier molecule.

Aside from these subtle details, the above experiments, which are designed to compare the bond strength, acidity, solvation, and H/D isotope exchange characteristics of proton-loaded zeolites with those of Brønsted acid zeolites, leave little ambiguity that ZOH′ and ZOH are for all of our immediate purposes to be considered as "identical".

Competitive Thermal Desorption (Dehydrohalogenation) Kinetic Study of HX and DX from $Na_{56}Y$

The main objectives of this solid-state kinetic investigation of the thermally induced dehydrohalogenation of HX and DX from $Na_{56}Y$ are to elucidate (i) the mechanism of the HX desorption process, (ii) details of the transition state for HX desorption, (iii) comparative HX desorption dynamics for α- and β-cage protons, (iv) dehydrohalogenation versus decationization (dehydroxylation) kinetics, and (v) cation and anion effects on the HX desorption process.

The experiments to be described were conducted on identical weight and equal thickness self-supporting wafers of $Na_{56}Y$, containing known and identical quantities of HX and DX (elemental analysis) corresponding to essentially eight hydrogen halide molecules per unit cell. This provides a starting mid-IR spectrum showing majority α-cage protonated and deuterated oxygen framework sites coexisting with very small but measurable quantities of similar β-cage sites (Figure 5). Solvation effects by HX are arranged to be at a minimal level (essentially no C band, see part 1). The temperature dependence of the dehydrohalogenation reaction in the range 100–200 °C was measured by monitoring the rate of loss of $\nu(OH_{\alpha,\beta})$ and $\nu(OD_{\alpha,\beta})$ in different $(HX)_8Na_{56}Y$ and $(DX)_8Na_{56}Y$ samples as well as in the same $(HX)_4(DX)_4Na_{56}Y$ sample. Some representative thermal desorption spectra are shown in Figure 5 from which it can immediately be discerned that $\nu(OD_\alpha)$ decays more rapidly than $\nu(OH_\alpha)$, implying the operation of an inverse kinetic isotope effect (KIE); see later.

(*i*) *Mechanism of the HX Desorption Process.* A proposed reaction pathway that was found to best fit the observed kinetic data and inverse KIE for the desorption of HX and DX from $Na_{56}Y$ is laid out in Scheme I.

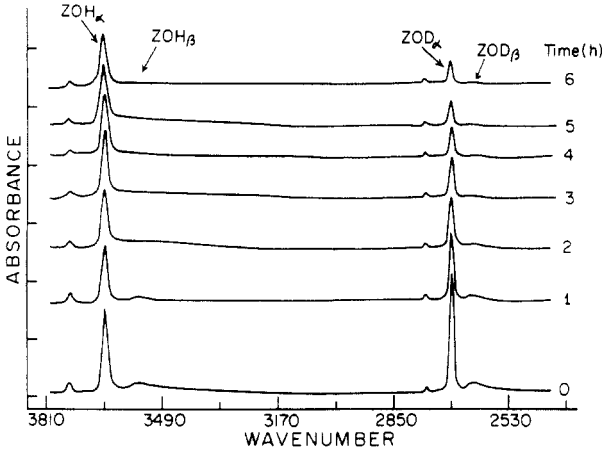

Figure 5. Competitive HX/DX/$Na_{56}Y$ thermal dehydrohalogenation kinetics recorded at 150 °C.

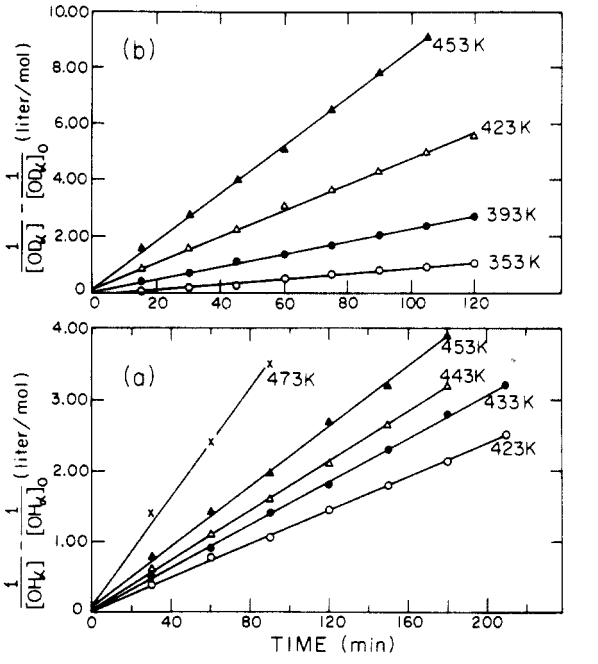

Figure 6. Bimolecular desorption kinetics for (a) HBr/$Na_{56}Y$ and (b) DBr/$Na_{56}Y$ in the temperature range 353–473 K.

SCHEME I

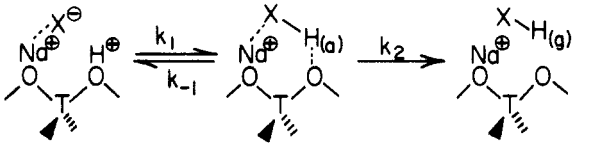

The assumptions in our kinetic model for dehydrohalogenation of HX involve (i) an α-cage located, weakly bound contact cation–anion pair denoted I, (ii) strict enforcement of 1:1 stoichiometry $[H^+] = [X^-]$, (iii) a rate-determining step (k_1) involving making a HX and breaking an OH bond, (iv) a low, steady-state concentration of short-lived $HX_{(a)}$ denoted II, (v) a fast $H{-}X_{(a)}$ desorption step (k_2) to $HX_{(g)}$ once the HX bond is made, denoted III, and (vi) a fast migration of protons between oxygen sites to the target desorption center denoted I (note that these protons could actually be near neighbors, making a diffusion term redundant).

In practice, the dehydrohalogenation kinetics are found to be well behaved and bimolecular (Figure 6) with an inverse KIE, $k_1^H/k_1^D \simeq 0.25$ measured at 150 °C.

(ii) Details of the Transition State for HX Desorption. The KIE expected for a late or productlike transition state involving making the HX/DX bond with little or no contribution from

TABLE I: Reaction Rate Data for the Dehydrohalogenation of $(HBr)_8Na_{56}Y$ and $(DBr)_8Na_{56}Y$ in the Temperature Range 353–473 K

	$(HBr)_8Na_{56}Y$		$(DBr)_8Na_{56}Y$	
T, K	10^4k_H, L mol^{-1} s^{-1}	$\Delta G_T^\ddagger$, kJ mol^{-1}	10^4k_D, L mol^{-1} s^{-1}	$\Delta G_T^\ddagger$, kJ mol^{-1}
353			1.5	115
393			3.7	125
423	1.9	137	7.7	133
433	2.4	140		
443	2.7	143		
453	3.7	145	14.0	140
473	5.3	150		

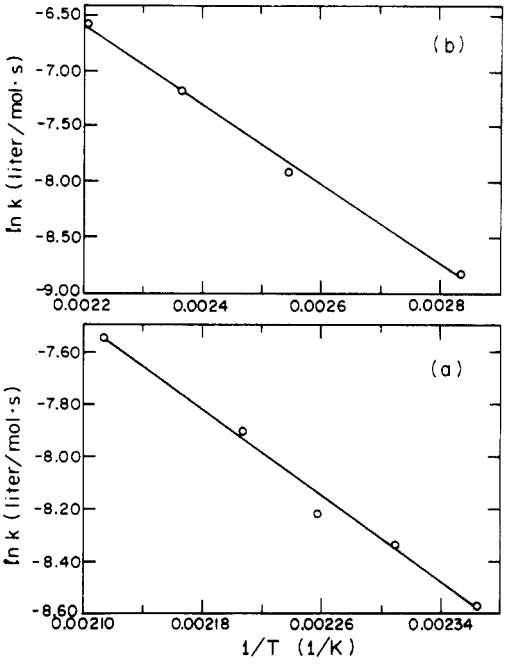

Figure 7. Arrhenius plots for the desorption of (a) HBr from HBr/$Na_{56}Y$ and (b) DBr from DBr/$Na_{56}Y$.

OH/OD bond breaking is expected from the difference in HX/DX zero-point energies to be $k_1^H/k_1^D \simeq 0.3$ at 150 °C.[7] The observed value of $k_1^H/k_1^D \simeq 0.25$ at 150 °C implies that a picture of the transition state can be envisioned to be like

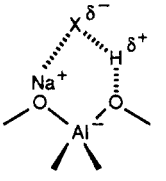

where mainly HX/DX bond making with little OH/OD bond breaking processes contribute to k_1. An Arrhenius plot of the temperature dependence of the k_1 rate data given in Table I (Figure 7) yields an activation energy for dehydrohalogenation of HBr and DBr: E_a(HBr) = 34.4 kJ mol^{-1} and E_a(DBr) = 30.1 kJ mol^{-1}, respectively (Table II).

In a thermodynamic treatment of the reaction rate data[7]

$$k_r = (kT/h)\exp(\Delta S^\ddagger/R)\exp(-\Delta H^\ddagger/RT)$$

for the dehydrohalogenation of HBr and DBr from $Na_{56}Y$ (Figure 8), one obtains the activation enthalpies and entropies, the values of which are given in Table II. The observed small positive enthalpy and the large negative entropy of activation for desorbing HBr or DBr from $Na_{56}Y$ strongly support the proposed mechanism in which two ions of opposing sign are brought together (possibly from near-neighbor framework oxygen sites) in a continuous

(7) Frost, A. A.; Pearson, R. G. *Kinetics and Mechanism*; Wiley: New York, 1961.

SCHEME II

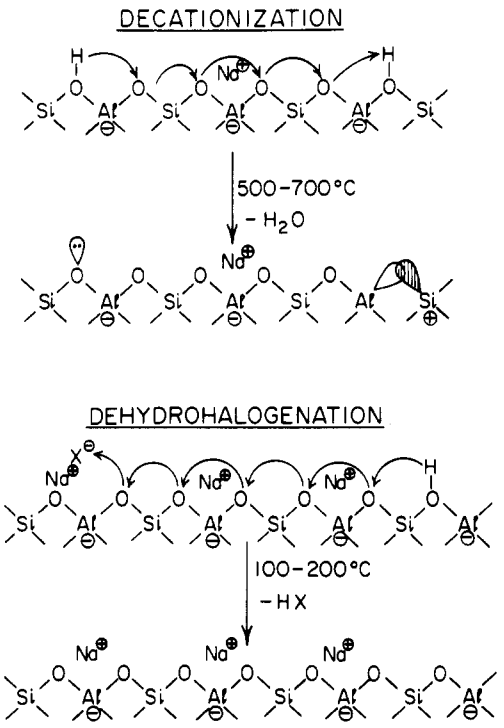

dielectric medium to form a neutral molecule (HX). In reactions involving ions, entropy often turns out to be the dominant factor compared to enthalpy, where Coulombic effects contribute to the enthalpy of the recombination process and a highly ordered transition state is responsible for the large decrease in the number of degrees of freedom of the system.[7] On the basis of the above information and space-filling considerations, a possible transition state for the desorption of HX from $Na_{56}Y$ is sketched in Figure 9.

(iii) Comparative HX Desorption Dynamics for α- and β-Cage Protons. Although these experiments were not intended to quantify the energetics and dynamics of α-cage versus β-cage dehydrohalogenations, one can readily discern from the measurements that $E_a^{\beta}(HBr) < E_a^{\alpha}(HBr)$ for $Na_{56}Y$. Thus, β-cage protonated oxygens begin to desorb at significantly lower temperatures (~100 °C) than those in the α-cage (~150 °C). Interestingly, this order is the microscopic reverse of the sequence in which they are formed from the sorption of HX into $Na_{56}Y$ (see earlier). Interproton and proton–cation repulsive interactions operating with the α- and β-cages for a particular proton–cation distribution must contribute to the energetics of the dehydrohalogenation process and hence the relative rates of loss of α- and β-cage protons for different cation types, populations, and distributions. This intriguing point is the topic of an ongoing study utilizing the series $HX/H_nM_{56-n}Y$ (where M = Li^+, Na^+, K^+, Rb^+, Cs^+).

(iv) Dehydrohalogenation versus Decationization Kinetics. In this section we wish to briefly direct attention to the similarity and differences between decationization (dehydroxylation, H_2O loss) of a Brønsted acid zeolite Y compared to the dehydrohalogenation (HX loss) of a proton-loaded zeolite Y. One striking difference is the temperature required to effect each of these processes, namely, around 500–600 °C for the former and 100–200 °C for the latter. Clearly there is a major difference between the energetics of decationization and dehydrohalogenation. The overall picture for decationization and dehydrohalogenation of zeolite Y is sketched in Scheme II.

It is apparent that in both schemes a proton has to move up to the target center to permit the eventual release of either H_2O or HX. Our decationization data (obtained at 500–600 °C) for both $H_8Na_{48}Y$ and $D_8Na_{48}Y$ display good bimolecular kinetic

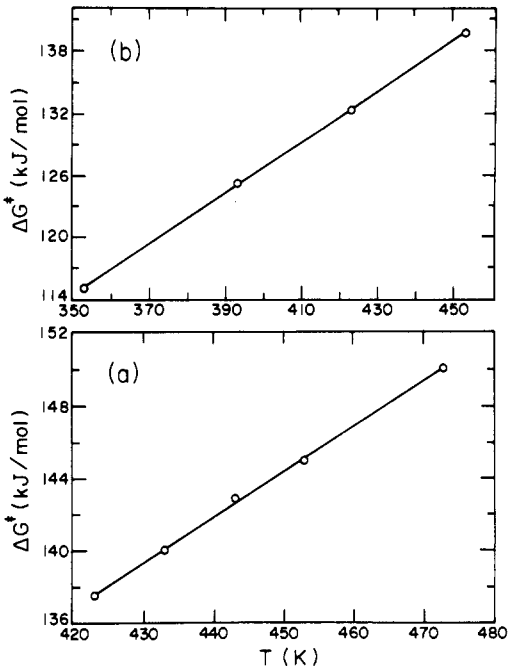

Figure 8. Thermodynamic treatment of the reaction rate data for the desorption of (a) HBr from $HBr/Na_{56}Y$ and (b) DBr from $DBr/Na_{56}Y$.

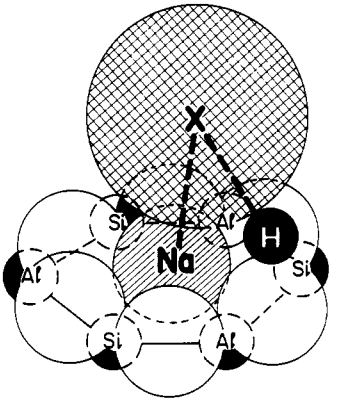

Figure 9. Proposed transition state for the dehydrohalogenation of HX from $Na_{56}Y$.

TABLE II: Arrhenius Activation Energies, E_a, Activation Enthalpies, $\Delta H^{\ddagger}$, and Activation Entropies, $\Delta S^{\ddagger}$, for the Dehydrohalogenation of $(HBr)_8Na_{56}Y$ and $(DBr)_8Na_{56}Y$ and the Decationization of $H_8Na_{48}Y$ and $D_8Na_{48}Y$

	E_a, kJ mol^{-1}	$\Delta H^{\ddagger}$, kJ mol^{-1}	$\Delta S^{\ddagger}$, J K^{-1} mol^{-1}
$(HBr)_8Na_{56}Y$	34.4	31.3	−251
$(DBr)_8Na_{56}Y$	30.1	30.1	−248
$H_8Na_{48}Y$	149.7	145.4	−159
$D_8Na_{48}Y$	145.7	141.1	−154

SCHEME III

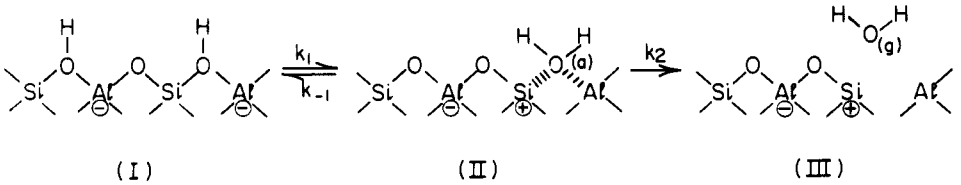

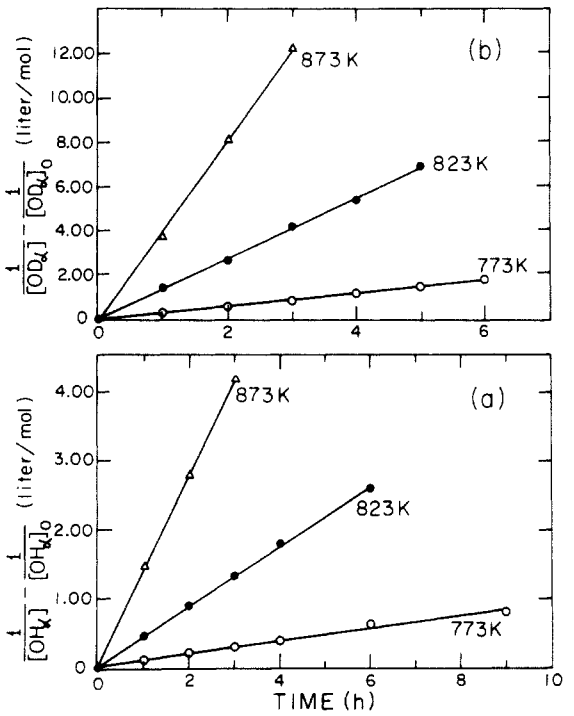

Figure 10. Bimolecular thermal decationization kinetics for (a) $H_8Na_{48}Y$ and (b) $D_8Na_{48}Y$ in the temperature range 773–873 K.

TABLE III: Reaction Rate Data for the Decationization of $H_8Na_{48}Y$ and $D_8Na_{48}Y$ in the Temperature Range 773–873 K

	$H_8Na_{48}Y$		$D_8Na_{48}Y$	
T, K	10^4k_H, L mol^{-1} s^{-1}	$\Delta G_T^{\ddagger}$, kJ mol^{-1}	10^4k_D, L mol^{-1} s^{-1}	$\Delta G_T^{\ddagger}$, kJ mol^{-1}
773	0.26	268	0.86	261
823	1.21	275	3.80	267
873	3.73	284	11.5	276

behavior (Figure 10) consistent with the picture illustrated in Scheme III.

Analysis of the data given in Table III (Figure 11) yields $k_1^H/k_1^D \sim 0.3$ with $E_a(D_2O) = 145.7$ kJ mol^{-1} and $E_a(H_2O) = 149.7$ kJ mol^{-1} (Table II). The activation enthalpies and entropies obtained from the thermodynamic treatment of the same data (Figure 12) are also listed in Table II. Clearly the sequence of events for decationization show a close parallel to those envisioned for dehydrohalogenation, but with some notable differences. First, production of the following transition states

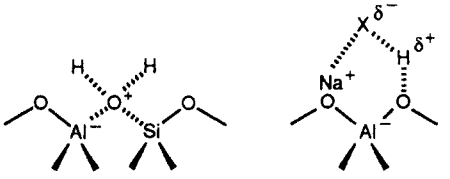

involve very different energetics. Decationization requires unfavorable proton–proton repulsions and disruption of T–O–T framework bonds, followed by release of water and creation of diamagnetic oxygen lattice defect sites. In contradistinction, dehydrohalogenation is envisaged to involve less destabilizing cation–proton repulsions and fragmentation of an OH bond, followed by release of HX. No wonder the activation energies and temperatures required for decationization of a Brønsted acid zeolite are so much greater than those required for dehydrohalogenation of a proton-loaded zeolite!

(v) *Cation and Anion Effects on the HX Desorption Process.* On considering the general form of the transition state envisioned for the dehydrohalogenation process in Figure 9, one can imagine how cation and anion variations are likely to effect the bond-making and bond-breaking processes that lead up to the formation of $HX_{(a)}$ and loss as $HX_{(g)}$. In this context it is worth noting that

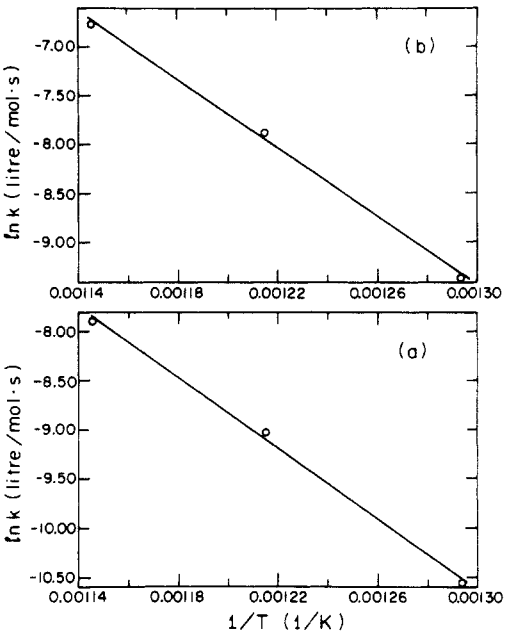

Figure 11. Arrhenius plots for the decationization of (a) $H_8Na_{48}Y$ and (b) $D_8Na_{48}Y$.

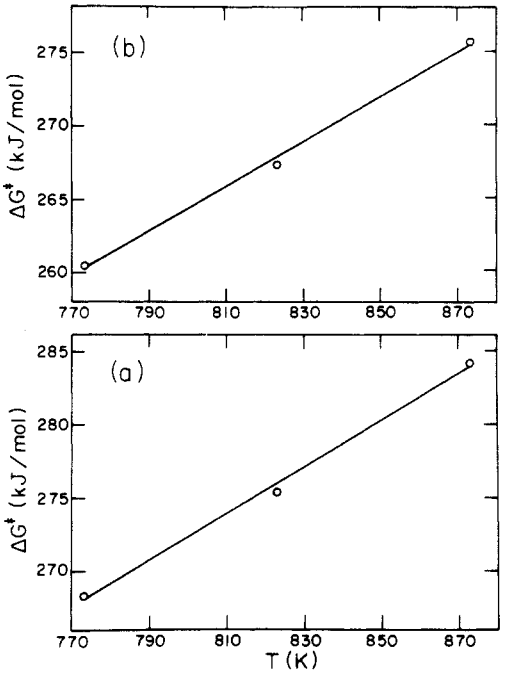

Figure 12. Thermodynamic treatment of the reaction rate data for the decationization of (a) $H_8Na_{48}Y$ and (b) $D_8Na_{48}Y$.

the observed invariance of the far-IR cation translatory modes to the adsorption/desorption processes of HX in $M_{56}Y$ implies that thermal or HX-induced migration effects of alkali-metal cations do not play an important role in proton-loaded zeolite Y.

Clearly the points that require addressing in order to gain an appreciation of the interplay of forces which likely control the energetics of this desorption process include (i) sensitivity of the OH bond strength to cation effects, (ii) the relative strengths of the HX bonds, and (iii) the sensitivity of the binding of the contact ion pair with respect to its cation and anion components.

Quantification of the contribution of anion and cation effects to the HX desorption process requires either detailed in situ kinetic measurements or temperature-programmed desorption data, yielding exact desorption temperature ranges and activation energies for each cation and anion type under investigation. These studies are under way. However, we can make an early step toward appreciating the effects at work by considering the temperatures (°C) at which (i) the α and β protonated oxygens begin

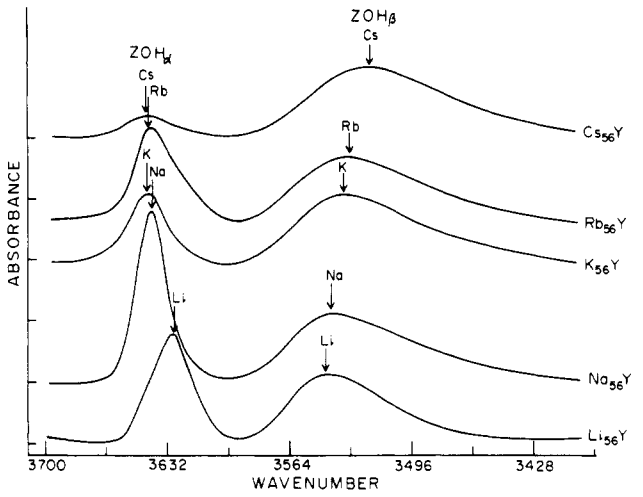

Figure 13. Cation effects on $\nu(OH_{\alpha,\beta})$ for $(HBr)_8M_{56}Y$ where M = Li, Na, K, Rb, Cs.

to yield observable losses denoted (T^{α}_{OH}, T^{β}_{OH}) and (ii) the solvated proton begins to release its hydrogen-bonded HX molecules denoted ($T_{(HX)_n}$) as laid out for the four cases studied so far and tabulated below:

$T_{OH}{}^{\alpha}$	$T_{OH}{}^{\beta}$	$T_{(HX)_n}$	M^+	X
100	70	40	Li	Br
150	120	100	Na	Cl
150	120	100	Na	Br
200	200	200	K	Br

The most striking points that emerge from this study are (i) there definitely exists a dramatic cation effect

$$T_{des}(K^+) > T_{des}(Na^+) > T_{des}(Li^+)$$

and (ii) compared to (i) the anion effect is insignificant

$$T_{des}(Br^-) \simeq T_{des}(Cl^-)$$

The cation effects are most easily comprehended in terms of the Sanderson average electronegativities S_{int} of the zeolite as discussed earlier:[3]

$$S_{int}(Cs_{56}Y) < S_{int}(Rb_{56}Y) < S_{int}(K_{56}Y) < S_{int}(Na_{56}Y) < S_{int}(Li_{56}Y)$$

This series implies that the order of lattice oxygen charge densities denoted ρ follows the order

$$\rho(Cs_{56}Y) > \rho(Rb_{56}Y) > \rho(K_{56}Y) > \rho(Na_{56}Y) > \rho(Li_{56}Y)$$

signaling that the OH bond strengths will also follow the latter order. This is indeed nicely reflected in the respective α-cage ν(OH) stretching frequencies observed for the protonated oxygen lattice sites

$$\nu(OH_\alpha)^{Cs} \gtrsim \nu(OH_\alpha)^{Rb} \gtrsim \nu(OH_\alpha)^{K} > \nu(OH_\alpha)^{Na} > \nu(OH_\alpha)^{Li}$$

as can be judged from Figure 13 and Table IV. It is worth mentioning that the trend of localizing the larger alkali-metal cations in the α-cage rather than the β-cage is probably responsible for the observed tendency for the $\nu(OH_\alpha)$ frequencies to level out after $K_{56}Y$ (Figures 13 and 14, Table IV). The origin of this effect is most likely proton–cation repulsions (steric factors) which will work in opposition to the effect of increasing oxygen framework charge densities (electronic factors) on passing from $Li_{56}Y$ to $Cs_{56}Y$.

With all of this information one can at last begin to appreciate why it is that dramatic cation effects are observed experimentally on the HX desorption kinetics. Thus, of the three zeolites studied so far in this way, $K_{56}Y$ boasts the most strongly bonded α-cage protonated oxygen framework site and the most strongly hydrogen-bonded proton! The acidities of these same protons as judged by their tendency to be solvated by HX (Figure 15) also display

TABLE IV: Mid-IR Spectra for $HX/H_nM_{56-n}Y$ in the ν(OH) and ν(XH) Stretching Region, where X = Cl, Br, I; M = Li, Na, K, Rb, Cs; n = 0–56[a]

system	A ($\nu(OH_\alpha)$)	B ($\nu(OH_\beta)$)	C[b]	D
$Li_{56}Y/HBr$	3631.2	3541.6	2850	2399
$Na_{56}Y/HCl$	3641.1	3544.3	2700	2375
$Na_{56}Y/HBr$	3642.1	3541.0	2850	2363
$Na_{56}Y/HI$	3643.1	3544.5	2900	2336
$K_{56}Y/HBr$	3643.6	3534.1	2833	2367
$Rb_{56}Y/HBr$	3644.0	3530.1	2853	2363
$Cs_{56}Y/HBr$	3644.6	3518.4	2845	2375
$H_{56}Y/HBr$	3638.9	3544.5	2966	2383
$H_{16}Na_{40}Y/HBr$	3642.7	3543.4	2880	2380
$H_8Na_{48}Y/HBr$	3644.3	3546.4	2854	2360

[a] All values in cm^{-1}. [b] The frequency of the C band depends upon the loading of hydrogen halide. The values quoted in the table refer to those for the zeolite saturated with hydrogen halide. Both the C and the D band are broad and structured (see part 1), rendering it difficult to pinpoint a precise frequency for their peak maxima.

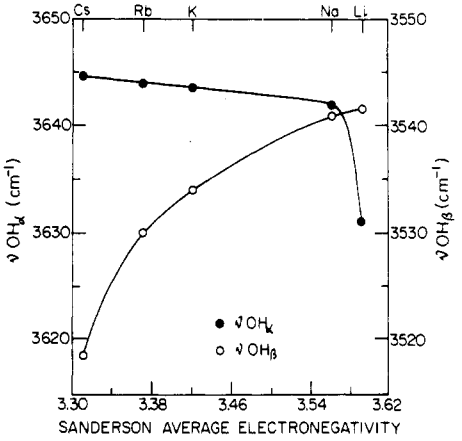

Figure 14. Cation dependence of the (a) α-cage and (b) β-cage ν(OH) stretching frequency in $(HBr)_8M_{56}Y$, where M = Li, Na, K, Rb, Cs.

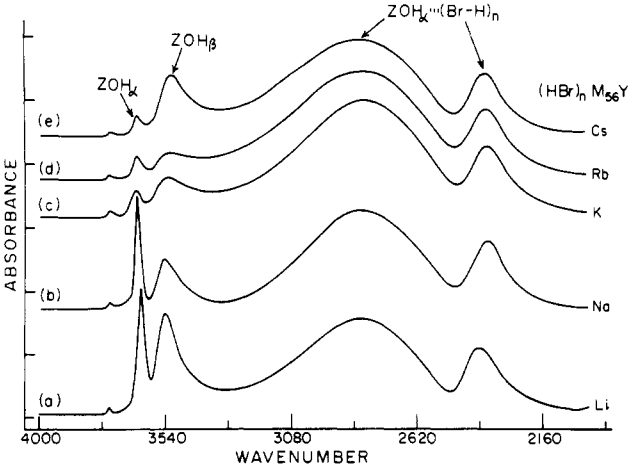

Figure 15. Representative series of mid-IR spectra for $(HBr)_nM_{56}Y$, where M = Li, Na, K, Rb, Cs.

a pronounced cation dependence, indicating that the acidities of $HX/M_{56}Y$ roughly parallel the order of OH bond strengths, namely

$$Cs^+ \sim Rb^+ \sim K^+ > Na^+ \sim Li^+$$

A vivid illustration of this increased tendency for proton solvation with increasing mass of the alkali-metal cation is illustrated for $K_{56}Y$ in Figure 15 where the equilibrium between HX protonation of the oxygen framework and proton solvation by HX clearly lies strongly toward the latter, when compared to the situation found for $HX/Na_{56}Y$ (see part 1, Figure 1). In this context it should be kept in mind that it is because of this increasing trend of proton solvation by $HX/Na_{56}Y$ (Figure 15) that it is not feasible to obtain

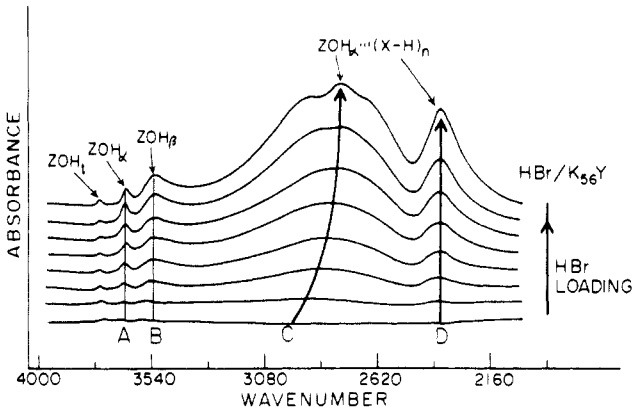

Figure 16. Mid-IR spectra of $HBr/K_{56}Y$ as a function of HBr loading.

the bathochromic $\Delta\nu_{OH}{}^{\alpha}$ shifts induced by weak bases like C_2H_6 or C_3H_6 (see earlier) to check the proposed order of acid strengths for $HX/M_{56}Y$ as a function of co-cation type. Also, the rather large breadth of the C band in the $HX/M_{56}Y$ series (Figure 15) renders it difficult to precisely pinpoint a peak maximum for the C band. As a result of this, it is not possible to draw meaningful conclusions about proton acidities from the bathochromic $\Delta\nu_{OH}{}^{\alpha}$ shifts by the HX molecule acting as the base or solvating moiety.

Before leaving the topic of cation effects, it is important to note that the anticipated trend of increasing ν(OH) stretching frequency of protonated alkali-metal zeolite Y with decreasing Sanderson electronegativity of the zeolite is *only* obeyed by the α-cage protons. In fact, precisely the opposite trend is observed for the β-cage protons (Figure 13). This dramatic turn of events alerts one to some of the limitations inherent in the Sanderson approach to zeolite electronegativities.[3] Recall that the model involves simple thermodynamic ideas which are able to provide relatively good qualification of inductive effects (for example, partial charge on constituent atoms). However, the model is somewhat constrained by the fact that there is no input of structure information and it is devoid of resonance, delocalization, or π-bonding effects. It should therefore not be too surprising to discover that the Sanderson electronegativity for zeolite Y is unable to simultaneously account for lattice oxygen charge density in both the α- and β-cages. However, this is a prerequisite for the successful discussion of α- and β-cage proton binding energies and $\nu(OH_{\alpha,\beta})$ stretching frequencies. One can deduce a posteriori from the observation of opposing frequency shifts for $\nu(OH_\alpha)$ (blue) and $\nu(OH_\beta)$ (red) on passing from Li^+ to Cs^+ that the known gradual migration of cations from the β-cage to the α-cage with increasing cation size in the alkali-metal cation series is reflected in a parallel depletion of oxygen framework charge density. That is, $S_{int}{}^{\alpha}$ decreases and $S_{int}{}^{\beta}$ increases on passing from $Li_{56}Y$ to $Cs_{56}Y$.

The apparent insignificance of any anion effect on the desorption process is presumably a manifestation of the weakly interacting nature of the cation–anion contact pair as proposed in part 1 of this study (e.g., small, α-cage specific, halide-induced far-IR shifts on the cation translational modes). Surprisingly, the HX bond strength order HCl > HBr > HI appears not to be playing an important role in the desorption process.

Conclusions

In brief, the key discoveries to emerge from this study are listed in point form below:

1. For proton-loaded zeolite Y $(HBr)_8Na_{56}Y$ and $(HBr)_8H_8Na_{48}Y$ compared to Brønsted acid zeolite Y $H_8Na_{48}Y$, vibrational, HX solvation, H/D exchange, and alkane acidity probes signal that the protons are for most purposes identical, having indistinguishable locations, bond strengths, acidities, and dynamics.

2. Competitive $HX/DX/Na_{56}Y$ desorption kinetics are well behaved and bimolecular with an inverse kinetic isotope effect, implicating an HX bond making process in the rate-determining step with a late (productlike) transition state.

3. A small positive enthalpy and large negative entropy of activation for the desorption of HBr from $Na_{56}Y$ are both in line with a dehydrohalogenation mechanism in which two ions of opposite sign H^+/X^- are brought together in a continuous dielectric medium to form a neutral HX molecule. Here Coulombic effects contribute to the enthalpy of the recombination process and a highly ordered transition state is responsible for the large decrease in the number of degrees of freedom of the system.

4. Cations display a dramatic effect while anions show an insignificant effect on the dehydrohalogenation energetics. The cation variations are manifest as changes in the α-cage oxygen framework charge density, OH bond strength, and proton–cation repulsions. The weakly bound nature of the cation–anion contact ion pairs and the absence of anion effects on the OH bond strengths are most likely at the origin of the observed weak anion effects on the desorption of HX from $Na_{56}Y$.

5. The activation energy for the bimolecular dehydrohalogenation of proton-loaded $(HBr)_8Na_{56}Y$ (34.4 kJ mol^{-1}) is considerably smaller than that for the bimolecular decationization (dehydroxylation) of Brønsted acid $H_8Na_{48}Y$ (149.7 kJ mol^{-1}). The former process involves the association of oppositely charged ions H^+/X^- to form a neutral HX molecule, leaving the lattice framework integrity intact. The latter process involves the association of protons on a single oxygen framework site and a transition state with large interproton repulsions. Subsequent loss of H_2O requires breaking Si–O/Al–O bonds with the formation of oxygen lattice vacancies and diamagnetic three-coordinate Al^{III}, Si^{IV} framework sites. Clearly dehydrohalogenation is considerably more facile than decationization.

Acknowledgment. We acknowledge the Natural Sciences and Engineering Research Council of Canada's Operating and Strategic Grants Programmes for generous financial support of this work. Invaluable technical discussions with and supplies of high-quality zeolites from Dr. Edith Flanigen at Union Carbide, Tarrytown, NY, proved to be especially worthwhile. L.M. acknowledges NSERC for a Summar Bursary, and S.O. expresses his gratitude to the Middle East Technical University for granting him an extended leave of absence to conduct his research at the University of Toronto. We also thank all of our co-workers at Toronto for many stimulating and enlightening discussions during the course of this work.

Registry No. HBr, 10035-10-6; HCl, 7664-39-3; HI, 10034-85-2; H_2, 1333-74-0; Li, 7439-93-2; Na, 7440-23-5; K, 7440-09-7; Rb, 7440-17-7; Cs, 7440-46-2.